# Nanoscale

Accepted Manuscript


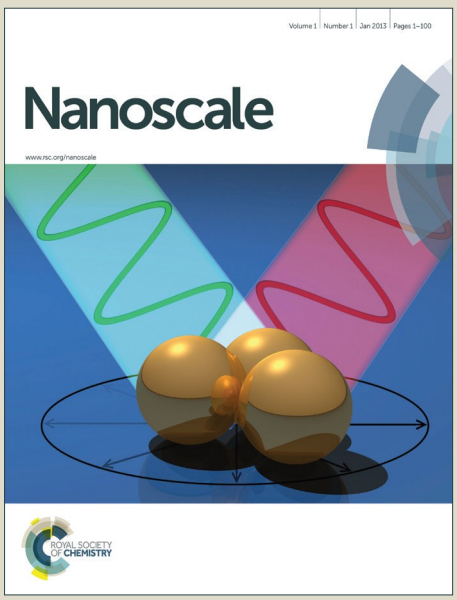





ROYAL SOCIETY OF CHEMISTRY

www.rsc.org/nanoscale

Journal Name

ARTICLE TYPE

Cite this: DOI: 10.1039/xxxxxxxxxx

# Ultrafast Charge-Transfer in Organic Photovoltaic Interfaces: Geometrical and Functionalization Effects†

Elton J. G. Santos,*[a,b,c] and W. L. Wang,[d,e‡]

Received Date
Accepted Date

DOI: 10.1039/xxxxxxxxxx

www.rsc.org/journalname

Understanding the microscopic mechanisms of electronic excitations in organic photovoltaic cells is a challenging problem in the design of efficient devices capable to perform sunlight harvesting. Here we develop and apply an *ab initio* approach based on time-dependent density functional theory and Ehrenfest dynamics to investigate photoinduced charge transfer in small organic molecules. Our calculations include a mixed quantum-classical dynamics with ions moving classically and electrons quantum-mechanically, where no experimental external parameter rather than the material geometry is required. We show that the behavior of photocarriers in zinc phthalocyanine (ZnPc) and $C_{60}$ systems, an effective prototype system for organic solar cells, is sensitive to the atomic orientation of the donor and the acceptor units as well as the functionalization of covalent molecules at the interface. In particular, configurations with the ZnPc molecules facing on $C_{60}$ facilitate charge transfer between substrate and molecule that occurs within 200 fs. In contrast, configurations where ZnPc is tilted above $C_{60}$ present extremely low carrier injection even at longer times as an effect of the larger interfacial potential level offset and higher energetic barrier between the donor and the acceptor molecules. An enhancement of the charge injection into the $C_{60}$ at shorter times is observed as binding groups connect ZnPc and $C_{60}$ in a dyad system. Our results demonstrate a promising way of designing and controlling at the atomic level the photoinduced charge transfer in organic devices that would lead to efficient carrier separation and maximize device performance.

## 1 Introduction

Organic photovoltaic solar (OPV) cells aim to provide a low-cost alternative to silicon based-solar cells[1–3]. Since abundant sources, chemical flexibility for modifications and easily handling manufacturing which allows inexpensive large-scale production, make OPV devices a subject of attracting attention. Nevertheless, their relatively low efficiency is one of the major challenges to be overcome. The key strategies to increase efficiency include improving total light absorption by using, for example, heterostructured materials. In such systems, compounds with complementary absorption spectra are combined which induce higher optical densities over a broader spectral range than at a single structure[4,5]. Other alternative is to design effective donor/acceptor (D/A) interfaces for electron-hole separation. Because excited states or excitons in organic materials present binding energy of several tenths of eV, this D/A interfaces can be designed to dissociate excitons into free electrons and holes as an effect of the energy offset between the two materials[5]. A promising example is the interface formed between $C_{60}$ and zinc phthalocyanines (ZnPc), which has shown efficiencies as higher as 2.2−6.0%[6–8]. Such small molecule solar cells producing considerable efficiency have become one of the most extensively studied systems for photovoltaic applications[2,3,9].

Recently, some mechanisms have been proposed to understand the effects of the local interactions on the rapid charge dissociation in this system and related polymer blends which happens at the femtosecond ($10^{-15}$s) timescale[10–13]. However, many questions remain at the interface that could be composed of ZnPc molecules at different stacking configurations[14–18], and how covalently bounded groups linking the donor and acceptors units are formed[19,20]. Moreover, extracting details of the photoin-

[a] *Department of Chemical Engineering, Stanford University, Stanford, California 94305, USA*
[b] *School of Mathematics and Physics, Queen's University Belfast, BT7 1NN, United Kingdom*
[c] *School of Chemistry and Chemical Engineering, Queen's University Belfast, BT9 5AL, United Kingdom; Tel: +44 028 9097 6044; Email: e.santos@qub.ac.uk*
[d] *Department of Physics, Harvard University, Cambridge, Massachusetts 02138, USA*
[e] *School of Engineering and Applied Sciences, Harvard University, Cambridge, Massachusetts 02138, USA*

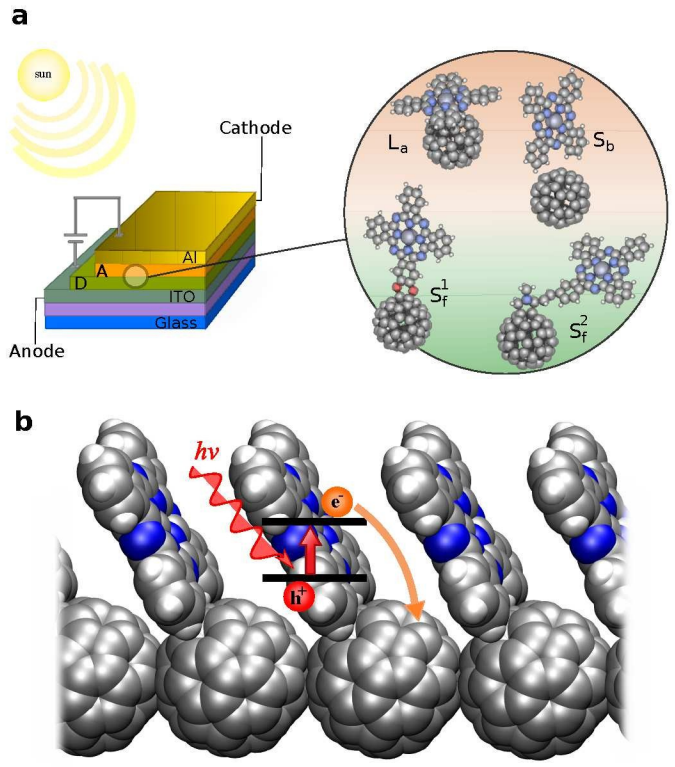


**Fig. 1** **a**, Molecular geometries for the ZnPc and $C_{60}$ across the donor/acceptor (D/A) interface in a photovoltaic experimental setup. Four different atomic structure are considered where: ZnPc lies down on top of $C_{60}$ surface ($L_a$); the molecule stays at a standing-up orientation on top of a bridge bond ($S_b$); a covalent functionalization mediated by O atoms upon carbon surface ($S_f^1$); similar to $S_f^1$ but using a 1,3-dipolar cycloaddition of azomethine ylides radical ($S_f^2$). **b**, Photoinduced charge transfer process in a $S_b$ D/A-interface. Photo absorption on ZnPc promotes an electron from its ground state to an excited state that is injected into the acceptor $C_{60}$ over a transition state barrier.

duced charge-transfer step, which is one of the most efficient process to suppress the Coulombic interactions between excited electron-hole pairs in specific and isolated donor-acceptor units, is not straightforward. Specifically, the microscopy mechanism of the charge generation and its detailed steps as well as the role of charge transfer (CT) states in the generation of free carriers has resulted to be controversial for many reasons[21]. Either in terms of the energy transfer provided by the charge transfer process that helps in the separation of CT states, or the electron delocalisation mediated charge-generation in polymer-fullerene interfaces. The high complexity of the samples and lack of methods to characterize the relative molecular orientations of donor and acceptor molecules at the interface[14] put limitations in further progress. In this context, a fully *ab initio* description of the main processes that govern the photoexcited charge transfer steps between $C_{60}$ and ZnPc, and their derivatives, as well as possible routes to increase the photocarrier generation in such organic systems has broad implications in understanding and designing such organic systems. At a more fundamental level, a coherent description of the charge migration from donor to acceptor is important for a general picture of photoinduced processes in OPV materials.

Here, we address photo-mediated charge transfer mechanisms at femtosecond regime of $C_{60}$ and ZnPc molecular complexes in various geometrical configurations, taking into account the effect of functionalization onto the $C_{60}$ surface by different organic groups. Geometrical configurations where ZnPc molecules lie flat on $C_{60}$, the face-on orientation, exhibit larger charge transfer than those where the molecules assume a tilted orientation, the edge-on geometry. The stronger electron polarization at the ZnPc/$C_{60}$ interface facilitates the charge injection from ZnPc into $C_{60}$ within 220 fs after excitation, which is rapid enough to escape the Coulomb trap where electron and holes form a close bound interfacial charge transfer state[5]. The photoexcitation process at face-on configurations is also eased by an interfacial electric field of $\sim$90 V/$\mu$m that is three times larger than that at edge-on geometries. The organic functionalization linking donor and acceptor at the interface plays a crucial role in the increase of the charge injection at shorter times. Oxygens or N-methylpyrrolidine groups covalently attached to the acceptor layer remove the tunneling barrier between both units and open an electronic channel for fast photocarrier transfer. Our results suggest the possibility to engineer different surface functionalization at D/A heterostructures for high organic-device efficiency.

## 2 Results

Figure **1a** shows the molecular structure of the models composed of ZnPc and $C_{60}$ molecules at D/A heterointerfaces in a photovoltaic setup. We investigated four representative adsorption geometries which ZnPc *i)* lying down on a C atom at the apex of two hexagons and one pentagon on $C_{60}$ (labeled $L_a$), *ii)* standing up above the bridge site between two C atoms of $C_{60}$ ($S_b$), *iii)* bounded to $C_{60}$ through two different covalent functionalizations using O adatoms ($S_f^1$) and *iv)* N-methylpyrrolidine group ($S_f^2$). The latter two configurations, $S_f^1$ and $S_f^2$, are also a class of dyad model where electron donor and acceptor molecules are covalently bound to each other. These atomic configurations are motivated by recent advances in producing atomically precise interfaces where the characterization and interfacial electronic structure have been reported by several experiments and calculations[19,20,22–29]. Indeed, a recent experimental correlation between molecular orientation at the donor-acceptor interface and important solar cell parameters, such as short-circuit voltage, fill factor, and dissociation rate, has been found. This points to a critical dependence of the device performance on its morphological features[14,15]. Therefore, we focus on the relative orientation between the molecules in more details.

To understand the charge separation at the D/A heterointerface (Fig. **1b**), we first analyze the electronic structure of each molecular configuration at the ground state. Figure **2a** shows the calculated total density of states (TDOS) as a function of the energy for $L_a$, $S_b$, $S_f^1$ and $S_f^2$ systems as well as the isolated $C_{60}$ and ZnPc molecules at LDA level (see *Methods* for details). With the adsorption of ZnPc on top of $C_{60}$, the highest occupied molecular orbital (HOMO) of the isolated systems, which was roughly at the same energy position (bottom of Figure **2a**), split by values in the range of 0.42−0.69 eV. This stabilizes the individual

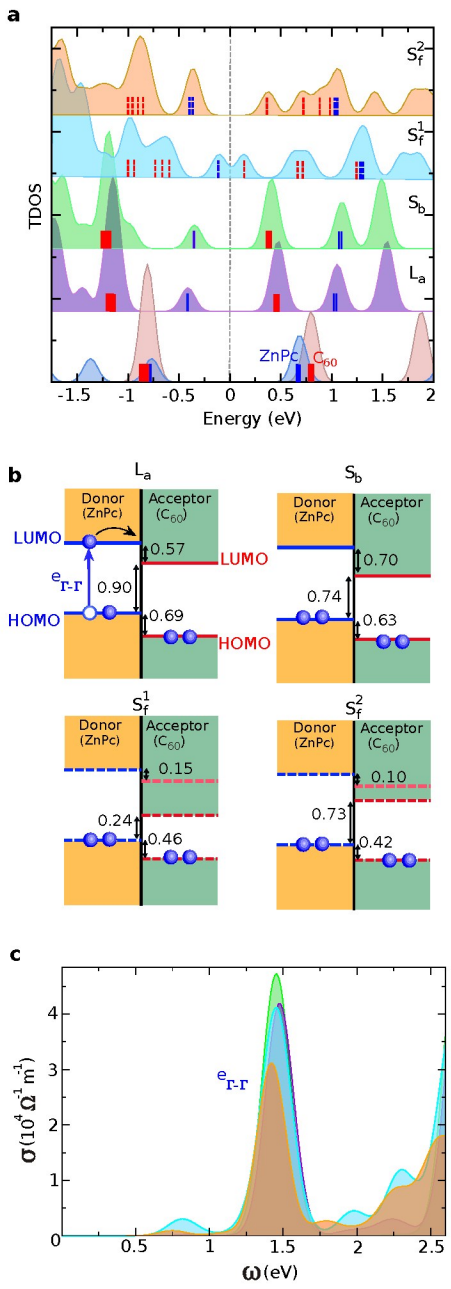


**Fig. 2** **a**, Calculated total density of states (TDOS) as a function of energy (in eV) of $C_{60}$ (faint red) and ZnPc (faint blue) molecules at the configurations $L_a$, $S_b$, $S_f^1$ and $S_f^2$ at the ground state. For clarity, curves for different D/A combinations have been shifted and smoothed with a Lorentzian broadening of 0.100 eV. The Fermi level is set to zero. The major contributions of each molecule, that is $C_{60}$ and ZnPc, on each interface around the Fermi level is marked by the vertical bars in blue and red colors. **b**, Energy level diagrams (eV) showing the main states involved in the photo-excitation dynamics at the Donor (ZnPc) and Acceptor ($C_{60}$) heterointerfaces. The HOMO and LUMO states are marked by the solid lines using the labeling in **a**. The corresponding transition between the HOMO and LUMO at the ZnPc molecule ($e_{\Gamma-\Gamma}$) is shown by means of the vertical arrow. At $L_a$, a scheme of the charge separation process at the D/A interface is shown (see text). **c**, Optical conductivity $\sigma$(in $10^4\ \Omega^{-1}m^{-1}$) as a function of the frequency $\omega$(in eV) of the four configurations of the ZnPc molecule on top of $C_{60}$ using the same colors as in **a**. The $e_{\Gamma-\Gamma}$ transition is marked by strong peak around ~1.35-1.51 eV.

HOMO's of $C_{60}$ and ZnPc to lower and higher energies, respectively, pinning the states of the phthalocyanine molecule at the Fermi level of the combined system (Figure 2**b**). A similar behavior is observed for the lowest unoccupied molecular orbital (LUMO), which is mainly composed of $C_{60}$ character. This is a common feature observed for each heterostructure with minor changes when chemical functionalization, as in $S_f^1$ and $S_f^2$, is included. In these two situations, states with character from the organic radical that bridges $C_{60}$ and ZnPc at the same molecular unit gives contribution to HOMO and LUMO which modify the initial degeneracy observed for the fullerene states (Figure 2**a**). These *bridge states* reduce the energy offset between the LUMO's at the D/A interface (Figure 2**b**) by as much as 0.47-0.58 eV in comparison with $L_a$ and $S_b$ configurations and offer well aligned carrier channels for electron-hole separation as discussed in more detail later.

We have also explicitly checked possible limitations on the exchange and correlation functional utilized in the chemical description of the energy levels shown in Fig. 2**b**. We have performed simulations taking into account a fractional component of the exact exchange from the Hartree-Fock (HF) theory hybridized with the DFT exchange-correlation functional at the level of the HSE06 hybrid functional[30] (see *Methods*) as shown in Figure 1S at the *Supporting Information*. We note that the overall description of the energy alignment presented in Fig. 2**a** is still consistent to higher levels of accuracy giving a fairly satisfactory representation of the interactions at the interface. It is important to remark, however, that quantitative differences at the orbital energies as large as 0.60 eV are present as most of the energies calculated using LDA are underestimated relative to HSE06. This suggests that the inclusion of the Fock exchange is an important ingredient in the energy-level alignment between the molecules once the interface is created. The excitation energy between HOMO and LUMO at ZnPc ($e_{\Gamma-\Gamma}$) also keeps a roughly constant value around ~1.41 eV for the different heterojunctions as shown in Figure 2**c**. This generates a well defined peak in the optical conductivity $\sigma$ (in $10^4\ \Omega^{-1}m^{-1}$) obtained in response to light with an electric field polarized along the molecular plane of the ZnPc molecule. This means that despite the different chemical configuration between ZnPc and $C_{60}$ the underlying optical response presents similar features.

The different energy alignment between ZnPc and $C_{60}$ molecular orbitals has its origin at the interfacial electrical dipole moment. Once the molecules stabilize the interface a net dipole as higher as 1.10 D, 0.70 D, 0.82 D and 3.60 D for molecular configurations $L_a$, $S_b$, $S_f^1$ and $S_f^2$, respectively, is formed. This generated a potential energy step across the interface that pulls up the ZnPc molecular orbitals relative to the carbon cage. The magnitude of the calculated dipole moments is consistent with the energy LUMO offset between ZnPc and $C_{60}$ band diagrams. The larger the interfacial dipole moment, the smaller the offset between the ZnPc and $C_{60}$ LUMO's (Figure 2**b**). This is in agreement with photoemission spectroscopy and ultraviolet photoelectron measurements performed on a similar structures involving CuPc and $C_{60}$ interfaces deposited on top of a metallic substrate[28]. In the case of $S_f^1$ and $S_f^2$ molecular structures, which the alignment with

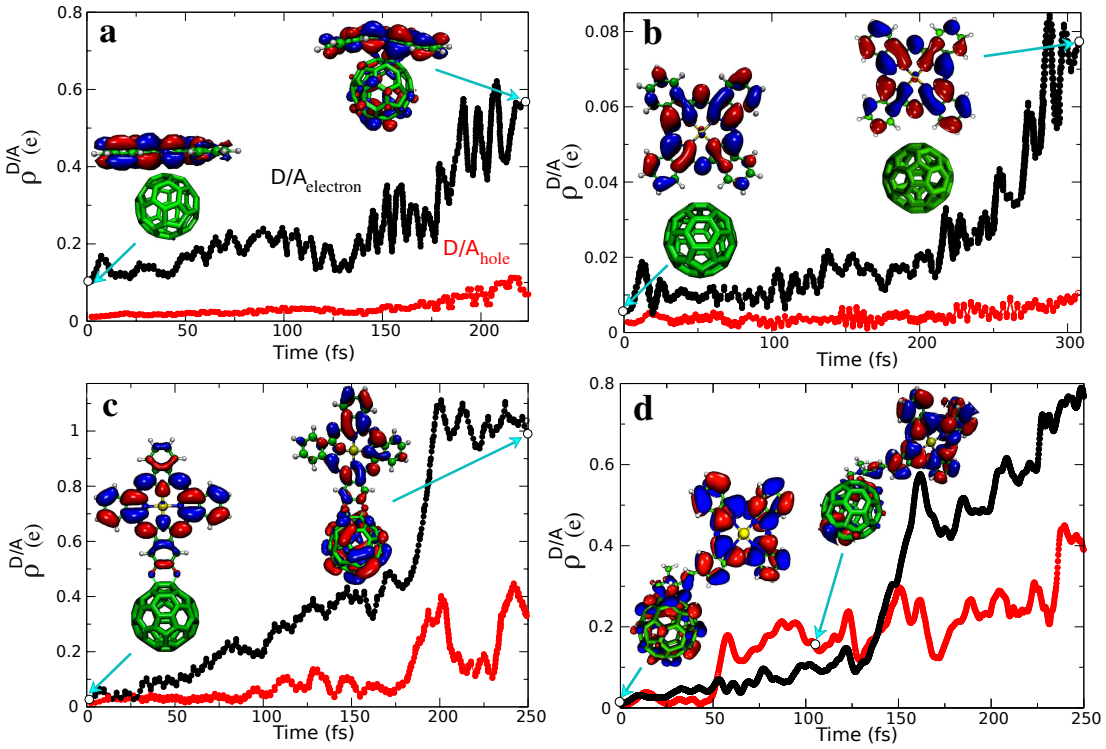


**Fig. 3** Time-dependent net charge $\rho^{D/A}$ (in electrons) on the $C_{60}$ molecule for the four D/A atomic arrangements: **a**, $L_a$, **b**, $S_b$, **c**, $S_f^1$ and **d**, $S_f^2$. The corresponding injection of electrons and holes into $C_{60}$ are defined by the black and red symbols, respectively. The excitonic wavefunctions (at $\pm 0.05$ $e^-$/Bohr$^3$) at initial ($t$ =0 fs) and later time ($t \geq 100$ fs) are shown in the insets in each panel. Blue and red isosurfaces are positive and negative values of the wavefunctions, respectively.

ZnPc LUMO is mediated by the bridge states, the energetic offset also follows this dipole moment rule but at smaller energy differences (∼0.1 eV).

In the following we focus on the excited state carrier dynamics on these ZnPc-$C_{60}$ interfaces, which play a central role in photovoltaic applications and daylight harvesting. We simulated this photocarrier dynamics as displayed schematically in Fig. 1**b** within the framework of the quantum-classical hybrid dynamics employing the Ehrenfest dynamics[31,32]. We first simulate the initial optical transition $e_{\Gamma-\Gamma}$ commented above (see Figure 2**c**) by promoting a valence electron at $t = 0$ from HOMO to LUMO in the first absorption band of ZnPc. This initial electronic structure is then evolved on time t> 0 over several femtoseconds within the time-dependent density functional formalism[33]. A full time dependent propagation of all the electronic states is performed by solving the time-dependent Kohn-Sham equations for the electrons. Ions are described classically through molecular dynamics based on Newton's classical equations of motion which are coupled to the electronic degree of freedom via the time-dependent electron density (see *Methods*). The interfacial electron-hole dynamics can be represented by the excess of charge on the acceptor $\rho^{D/A}$ (in electrons) which is calculated from the time evolution of the molecular orbital of interest. In this process, two-electron Coulomb coupling of exciton transfer are not taken into account as the direct competition with charge transfer states created at the interface is not the focus of this work[34]. We calculate instead an one-by-one electron and hole transfer between the two molecules at the energy limited by their frontier orbitals (HOMO, LUMO). Other theoretical approaches using quantum-chemistry methods, such as MS-CASPT2, fragment excitation-difference, and configuration interaction, would be more suitable to be used as the exciton-charge coupling is explicitly included at a considerable computational cost[35–37].

Figure 3 shows that after the photoexcitation occurs, there is a considerable electron-hole separation in the $L_a$, $S_f^1$ and $S_f^2$ configurations but a negligible charge transfer in the $S_b$ molecular geometry. The former three configurations show an electron injection into the acceptor on a time scale of 190−250 fs. These values agree well with those found using time-resolved two-photon photoemission measurements[10] and femtosecond time-resolved second harmonic generation[38]. We note that the time scale observed for $L_a$, $S_f^1$ and $S_f^2$ geometries is one order of magnitude higher than that present at edge-on $S_b$ system which show substantial modifications of their wavefunction isosurfaces at different times (see snapshots of selected excitonic state charge distributions in Figure 3). This is in remarkable agreement with recent spectroscopy measurements and calculations for a different $C_{60}$-based organic interface[39,40] and suggests a general role of the effect of the D/A geometry on the excited electron-hole dynamics.

Furthermore, the hole dynamics is much slower than that of the excited electron and is observed only at times when the excited electron is at least half transferred, $\rho^{D/A} \sim 0.5$ electrons, to the $C_{60}$ molecule. This effect is observed clearly at $S_f^1$ configuration

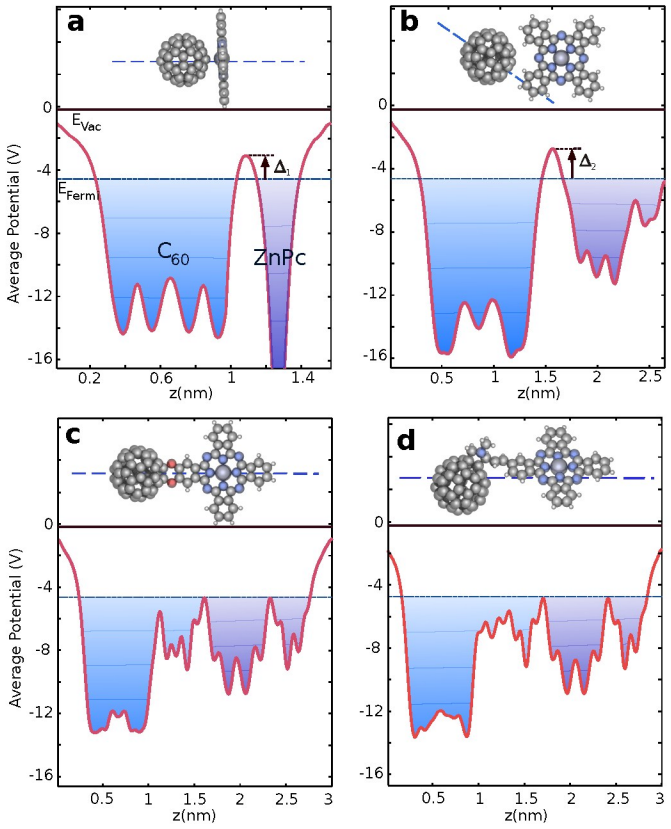


**Fig. 4** Total average potential cross section for the different configurations between $C_{60}$ and ZnPc: **a**, $L_a$, **b**, $S_b$, **c**, $S_f^1$ and **d**, $S_f^2$. The chosen path along which the average was performed is shown by the dashed line in the inset above every potential. The vacuum level ($E_{Vac}$) and the Fermi level ($E_{Fermi}$) are marked by the horizontal solid and dashed lines, respectively. The energetic barriers $\Delta_{1,2}$ in **a**, and **b**, are shown by the vertical arrows in relation to $E_{Fermi}$.

(Figure 3**c**) at $t = 185$ fs, which shows an increasing of 10 times of the hole contribution in comparison to earlier evolution times. This suggests that the electron-hole interaction could play a role on the hole transfer into the acceptor due to the finite size of the molecule. We also observed that the amount of photoexcited carriers transferred to the $C_{60}$ molecule is enhanced on the $S_f^1$ and $S_f^2$ configurations in comparison with $L_a$ and $S_b$. At $t$ =250 fs, the excited electron is completely injected into the acceptor for the two functionalized structures, indicating that a faster electron-hole dissociation process occurs through the binding groups that covalently link donor and acceptor. This is in agreement with optical measurements performed for phthalocyanine-fullerene dyad compounds that have shown efficient photoinduced electron transfer in covalent ZnPc-$C_{60}$ systems[41–46].

It is worth mentioning that charge transfer occurring on the 200 fs timescale is significantly faster than the exciton lifetime for the ZnPc-$C_{60}$ interface as recently measured using transient absorption and time-resolved terahertz spectroscopy[22]. Therefore, even the very slowest configuration presented in this work, that is, $S_b$, would still out-compete exciton recombination. One of the major photo-physical factors that limits device performance is the recombination of free carriers[17,47–49]. Both recombination and charge transport/extraction (not studied here) from the photovoltaic device that compete on the microsecond timescale are very sensitive to small changes in the recombination lifetime[5]. The specific geometrical and electronic structure that assists exciton dissociation is observed in our calculations to induce modifications on the Coulombic interactions of the excited electron-hole pairs. The consequent transport of the light-excited carriers from the D/A interface to the electrodes (anode and cathode), which may also depend on the proper geometry of the electron and hole transport layer, still remain elusive. Since no donor-to-donor interactions at excitation level (interfacial charge transfer state)[10] have been taking into account in our model due to the many-body nature of the electron-hole interactions.

The main differences observed in the excited dynamics for the different molecular structures can be understood through the interfacial level alignment as discussed above and the total potential as shown in Figure 4. At molecular structures where the donor ZnPc component is not fixed to the acceptor $C_{60}$, that is, the $L_a$ and $S_b$ systems, a energetic barrier ($\Delta$) of $\Delta_1 \sim$1.40 eV and $\Delta_2 \sim$2.05 eV, respectively, prevents the electron to tunneling from ZnPc to $C_{60}$ at the ground state (Figure 4**a**,**b**). Once the system is photoexcited by the energy needed to generated the optical transition $e_{\Gamma-\Gamma}$ from HOMO to LUMO of ZnPc (Figure 2) the excited electron has enough energy to overcome that barrier, and in the case of $L_a$ configuration an electron transfer is observed. For $S_b$ geometry, the higher barrier in comparison to $L_a$ configuration and the larger energy offset between the LUMO states at the D/A interface (see Figure 2**b**) suppresses the photocarrier injection into the $C_{60}$ acceptor at the excitation energy utilized. The $S_b$ configuration is also the most unlikely to be observed in interfaces as recently measured by ion-mass spectrometry[28]. Moreover, the photoexcitation process at face-on $L_a$ configuration is eased by an interfacial electric field of $\sim$90 V/$\mu$m that is three times bigger than that at edge-on geometries. Interfacial electric-field driven photoinduced charge transfer at similar systems has recently been measured using femtosecond time-resolved second harmonic generation which is in close agreement with our results[38].

The photoexcitation electron transfer is also efficient in covalently functionalized ZnPc-$C_{60}$ structures, e.g. $S_f^1$ and $S_f^2$, as discussed above but with the main advantage that a barrierless potential exists at the D/A interface (Figure 4**c**-**d**). This indicates an electronic communication between both molecular units in the ground state similarly to that observed in electrochemical characterization[19,50,51]. In this regard, the chemical radicals that anchor ZnPc and $C_{60}$ to the same electroactive unit establish an open channel which enables electron and hole injection into the D/A interface. Indeed, the $S_f^1$ and $S_f^2$ configurations show the highest hole transfer ($\rho^{D/A} \sim 0.45$ electrons at $t$ =240 fs) among the studied geometries which indicates that if the electron-hole recombination may happen at longer times (not shown here) at the acceptor unit, the efficiency of the solar-cell devices based on this dyad might be rather low. This behavior is in agreement with electrical-optical experiments[42] where a low power conversion efficiency was estimated for ZnPc-$C_{60}$ dyads.

## 3 Conclusions

We have considered the interplay between photocarrier dynamics and structural and functionalization factors at D/A interfaces as a fundamental issue in the design of efficient organic photovoltaic devices. Our *ab initio* approximations have provided an atomic-scale description of the exciton dynamics at ultrafast time-domain on ZnPc-$C_{60}$ systems, as well as microscopic detail of the interfaces that are difficult to extract from experiments, such as the potential barriers. Our results show that configurations where ZnPc molecules lay down on top of $C_{60}$ carbon structure[52], or binding groups covalently connect ZnPc and $C_{60}$ in a single electroactive unit, facilitate the excited electron injection into the acceptor. The excitation process occurs in a timescale of ∼190-250 fs, which is helped by lower interfacial energetic barriers on face-on geometries and barrierless behavior for functionalized heterojunctions. Covalent functionalization improves the photoelectron transfer at the interface but with the cost of the increasing of the unwanted hole transfer due to the electronic coupling between donor and acceptor. This functionalization effect based on the tuning of the interfacial potential barriers that mediate efficient photoinduced carrier dynamics adds an additional degree of freedom in the understanding and design of organic interfaces for sunlight harvesting, which may guide to new avenues of effective electron-hole separation mediated by engineering chemical groups at the interface.

## 4 Acknowledgments

We thank Charles Black, David R. Reichman, Konstantinos Fostiropoulos, Chia Wei Hsu, Paul Weiss, James Hone and Philip Kim for valuable discussions. E.J.G.S. acknowledges the use of computational resources from the UK national high performance computing service, ARCHER, for which access was obtained via the UKCP consortium and funded by EPSRC grant ref EP/K013564/1; and the Extreme Science and Engineering Discovery Environment (XSEDE), supported by NSF grants number TG-DMR120049 and TG-DMR150017. The Queen's Fellow Award through the startup grant number M8407MPH is also acknowledged.

## 5 Methods

The simulations reported here are based on density functional theory calculations using the SIESTA method[53] and the VASP code[54,55]. The localized density approximation[56] along with non-local van der Waals density functional for the exchange-correlation term[57] have been used. A double-$\zeta$ polarized basis set in SIESTA, and a well-converged plane-wave cutoff of 400 eV in VASP were utilized in the calculations. Projected augmented wave method (PAW)[58,59] for the latter, and norm-conserving Troullier-Martins pseudopotentials[60] for the former, have been used in the description of the bonding environment at the different geometrical configurations between $C_{60}$ and ZnPc molecules. Atomic coordinates were allowed to relax until the forces on the ions were less than 0.04 eV/Å under the conjugate gradient algorithm. Further relaxations (0.01 eV/Å) do not change appreciably the energetics and geometries.

To avoid any interactions between supercells in the non-periodic direction, a 15 Å vacuum space was used in all calculations. In addition to this, a cutoff energy of 150 Ry was used to resolve the real-space grid used to calculate the Hartree and exchange-correlation contribution to the total energy. A basis set of numerical atomic orbitals obtained from the solution of the atomic pseudopotential at slightly excited states as implemented in the SIESTA[53] code was used. We have utilized an *energy shift* of 50 meV to define the radii of different orbitals. We have also carried out calculations using screened hybrid functionals at the level of Heyd-Scuseria-Ernzerhof (HSE06) approach[30]. In this approximation part of the short range exchange energy is replaced by a portion of exact Hartree-Fock exchange energy. Here we used HSE06 as an example of a hybrid functional because of its successful applications in solids and molecules[61–63], and because of its less expensive computational cost to treat the slow-decaying long-range part of the exchange interaction in comparison to the PBE0 functional[64].

To perform the fully quantum-mechanical simulations of the of electron-hole dynamics as well as the time evolution of the charge transfer for the different systems, we use Konh-Sham (KS) scheme within TDDFT[33] using the localized basis set algorithm implemented in SIESTA. The TDDFT is a *state-of-art* first-principles approach for the treatment of the linear and nonlinear response of optical excitations in molecules, cluster and extended systems[65–68]. The time-dependent electron density is given by $\rho(\mathbf{r},t)=\sum_j|\Psi_j(\mathbf{r},t)|^2$ with the summation running over all occupied states. The evolution of the system is determined by solving the time-dependent KS equation for single-particle orbitals $\Psi_j(\mathbf{r},t)$:

$$i\hbar\frac{\partial\Psi_j(\mathbf{r},t)}{\partial t}=H\Psi_j(\mathbf{r},t) \tag{1}$$

where $H$ is the time-dependent Hamiltonian of the system

$$H=-\frac{\hbar^2}{2m}\nabla^2_{\mathbf{r}}+\int\frac{\rho(\mathbf{r}',t)}{|\mathbf{r}-\mathbf{r}'|}d\mathbf{r}'-\sum_i\frac{Z_i}{|\mathbf{r}-\mathbf{R}_i|}+v_{xc}[\rho(\mathbf{r},t)]+v_{ext}(\mathbf{r},t) \tag{2}$$

where the first term is the kinetic energy of electrons, the second term is the Hartree potential, the third term is electron-ion interaction, the fourth term $v_{xc}$ is the exchange-correlation potential treated at LDA level, and the fifth term $v_{ext}$ is an external perturbation. We considered the external potential due to the light source as $v_{ext}=-\mathbf{E}_{ext}(t)\cdot\mathbf{r}$, where $\mathbf{E}_{ext}(t)=A_0\hat{z}\delta(t)$ is a short duration external electric field polarized along the z-axis. We have set the value of $|\mathbf{E}_{ext}|$ within $0.001-0.01$ eV/Å. The electron-hole excitations are modeled by swapping the occupation of the KS eigenvalues, $\Psi_j^{E+h\nu}(\mathbf{r},t)$, involved in the excitation process. This is equivalent to consider vertical transitions from the ground state to an excited state which take place instantaneously at $t=0$ by the absorption of a single photon[31,69,70]. This is a good approach of the excited states included in a photoexcitation process as successfully used in several systems[69,71–73]. We find that Γ-point sampling in the Brillouin zone (BZ) is enough to describe the coupling between ionic and electronic degrees of

freedom through the one-by-one electron and hole transfer at the D/A interface.

We simulate the excited-state dynamics by turning on the external potential $v_{ext}$ at $t = 0$, and propagating the occupied KS state $\Psi_j^{E+h\nu}(\mathbf{r},t)$ by solving Eq.(1) at later times $t > 0$ with $v_{ext} = 0$. The solution of KS equation for electrons is given by[32]:

$$\Psi_j(\mathbf{r},t+\Delta t) = \hat{U}(t+\Delta t,t)\Psi_j(\mathbf{r},t) \quad (3)$$

$$\hat{U}(t+\Delta t,t) = \hat{T}exp\left(-\frac{i}{\hbar}\int_t^{t+\Delta t} H(s)ds\right) \quad (4)$$

where $\hat{U}$ and $\hat{T}$ are the time-evolution and the time-ordering operators, respectively. We can approximate the exponential form of $\hat{U}(t+\Delta t,t)$ by a Crank-Nicolson operator[74]. The electronic density is updated self-consistently during the real-time propagation of $\Psi_j(\mathbf{r},t)$ with a time step of $\Delta t$ =0.02419 fs. The total energy is conserved to within $10^{-5}$ eV/fs per atom giving a variation of the total energy of less than 0.1 eV, which is comparable to errors from other methods. The dynamics of the ions is treated classically within the Ehrenfest method. The ions are allowed to move following a classical molecular dynamics under the influence of the quantum forces due to the electrons. These forces are derived in the mean-field approximation as the derivatives of the total energy with respect to ionic positions via the Hellmann-Feynman theorem:

$$\sum_j \nabla_{\mathbf{R}}\langle\Psi_j|\frac{Z}{|\mathbf{R}-r|}|\Psi_j\rangle \approx \sum_j \langle\Psi_j|\nabla_{\mathbf{R}}\frac{Z}{|\mathbf{R}-r|}|\Psi_j\rangle \quad (5)$$

In this approximation, ions evolve on an effective potential describing an average over several possible adiabatic energy states which are weighted by their occupation probabilities. After evaluating all the forces on each atom, we carry out the molecular-dynamics simulation for the ions with the new ionic position $\mathbf{R}_{l+1}$ and velocities $\mathbf{v}_{l+1}$ at time $t_{l+1} = (l+1)\Delta t$ are calculated using the Verlet algorithm[75]:

$$\mathbf{R}_{l+1} = \mathbf{R}_l + \mathbf{v}_l\Delta t + \frac{\mathbf{F}_l(\Delta t)^2}{2M} \quad (6)$$

$$\mathbf{v}_{l+1} = \mathbf{v}_l + \frac{(\mathbf{F}_l + \mathbf{F}_{l+1})\Delta t}{2M} \quad (7)$$

The initial velocities at $t = 0$ are assigned according to the equilibrium Maxwell-Boltzmann distribution at a given temperature of 350K unless otherwise specified. Both initial ground state and subsequent excited-state calculations have been performed using LDA approach as it gives consistence on the solution of the Kohn-Sham equations at both levels of the theory, without the inclusion of energy differences if a different functional is used in a previous calculation. Indeed, quantitatively capturing charge-transfer states with DFT is nontrivial, and different approximations have been used for several groups. For instance, in terms of range-separated hybrid functionals[28,76,77] to correctly describe frontier orbitals, ionization potentials, electron affinities in terms of optimally tuned switching parameters. Such approach has shown to improve the description of several orbital energies of gas phase molecules important to photovoltaic applications, where agreement with experimental measurement is achievable. However, a fully excited-state hybrid functional dynamics for systems with hundred of atoms in the unit cell is prohibitive as these calculations are heavily time-consuming. The average potential profiles were calculated by averaging the potentials at the points within a cross section along the given axis. An amplitude cutoff of -1V was used to exclude the vacuum area from the averaging for all profiles.

The calculation of the optical properties was based on the computation of the complex dielectric function $\varepsilon(\omega) = \varepsilon_1(\omega) + i\varepsilon_2(\omega)$, in which the imaginary part $\varepsilon_2(\omega)$ is given by

$$\varepsilon_2(\omega) = \frac{e^2\hbar}{\pi m^2\omega^2}\sum_{i,j}\int_{\mathrm{BZ}} d\mathbf{k}|W_{ij}(\mathbf{k})|^2\delta[\omega - \omega_{ij}(\mathbf{k})] \quad (8)$$

where the integral is over all $\mathbf{k}$-points in the Brillouin zone (BZ) and the sum runs over all possible pairs of valence $|\phi_i\rangle$ and conduction $|\phi_j\rangle$ bands with corresponding eigenvalues $E_i$ and $E_j$, such that $\hbar\omega_{ij}(\mathbf{k}) = E_j - E_i$. The electric dipole transition matrix element $W_{ij}(\mathbf{k})$, which represents the transition rate of an electron from state $|\phi_i\rangle$ to state $|\phi_j\rangle$, is given by $W_{ij}(\mathbf{k}) = \langle\phi_j(\mathbf{k})|\hat{\mathbf{e}}\cdot\mathbf{p}|\phi_i(\mathbf{k})\rangle$, with $\hat{\mathbf{e}}$ and $\mathbf{p}$ being the polarization vector and the momentum operator, respectively. The optical conductivity is given by $\sigma(\omega) = (\omega/4\pi)(\varepsilon_2(\omega) - 1)$[78]. We found the dielectric function and optical conductivity to be sufficiently well converged with a mesh of $30\times30\times1$ $k$ points. A Gaussian broadening of 100 meV was used to plot the optical conductivity as a function of the frequency.

## References


1 H. Hoppe, N. S. Sariciftci, *J. Mater. Res.* 2004, **19**, 1924-1945.

2 M. Riede, T. Mueller, W. Tress, R. Schueppel, K. Leo, *Nanotechnology* 2008, **19**, 424001-424013.

3 A. Hadipour, B. de Boer, P. W. M Blom, *Adv. Funct. Mater.* 2008, **18**, 169-181.

4 C. W. Tang, *Appl. Phys. Lett.* 1986, **48**, 183-188.

5 T. M. Clarke, J. R. Durrant, *Chem. Rev.* 2010, **110**, 6736-6767.

6 I. Bruder, M. Karlsson, F. Eickemeyer, J. Hwang, P. Erk, A. Hagfeldt, J. Weis, N. Pschirer, *Sol. Energy Mater. Sol. Cells* 2009, **93**, 1896-1899.

7 Z. R. Hong, B. Maennig, R. Lessmann, M. Pfeiffer, K. Leo, P. Simon, *Appl. Phys. Lett.* 2007, **90**, 203505-203509.

8 W. Zeng, K. S. Yong, Z. M. Kam, F. Zhu, Y. Li, *Appl. Phys. Lett.* 2010, **97**, 133304-133308.

9 J. Xue, B. P. Rand, S. Uchida, S. R. Forrest, *Adv. Mater.* 2005, **17**, 66-71.

10 A. E. Jailaubekov, A. P. Willard, J. R. Tritsch, W. L. Chan, N. Sai, R. Gearba, L. G. Kaake, K. J. Williams, K. Leung, P. J. Rossky, X. Y. Zhu, *Nat. Mater.* 2013, **12**, 66-73.

11 G. Grancini, M. Maiuri, D. Fazzi, A. Petrozza, H. J. Egelhaaf, D. Brida, G. Cerullo, G. Lanzani, *Nat. Mater.* 2013, **12**, 29-

33.
12 A. A. Bakulin, A. Rao, V. G. Pavelyev, P. H. M. van Loosdrecht, M. S. Pshenichnikov, D. Niedzialek, J. Cornil, D. Beljonne, R. H. Friend, *Science* 2012, **335**, 1340-1344.
13 S. Gélinas, A. Rao, A. Kumar, S. L. Smith, A. W. Chin, J. Clark, T. S. van der Poll, G. C. Bazan, R. H. Friend, *Science* 2014, **343**, 512-516.
14 J. R. Tumbleston, B. A. Collins, L. Yang, A. C. Stuart, E. Gann, W. Ma, W. You, H. Ade, *Nat. Photon.* 2014, **8** , 385-391.
15 B. P. Rand, D. Cheyns, K. Vasseur, N. C. Giebink, S. Mothy, Y. Yi, V. Coropceanu, D. Beljonne, J. Cornil, J. L. Bredas, J. Genoe, *Adv. Funct. Mater.* 2012, **22**, 2987-2995.
16 K. R. Graham, C. Cabanetos, J. P. Jahnke, M. N. Idso, A. El Labban, N. Ngongang, T. Heumueller, K. Vandewal, A. Salleo, B. F. Chmelka, A. Amassian, P. M. Beaujuge, M. D. McGehee, *J. Am. Chem. Soc.* 2014, **136**, 9608-9618.
17 M. Schubert, B. A. Collins, H. Mangold, I. A. Howard, W. Schindler, K. Vandewal, S. Roland, J. Behrends, F. Kraffert, R. Steyrleuthner, Z. Chen, K. Fostiropoulos, R. Bittl, A. Salleo, A. Facchetti, F. Laquai, H. W. Ade, D. Neher, *Adv. Funct. Mater.* 2014, **24**, 4068-4081.
18 W. Chen, D. C. Qi, H. Huang, X. Gao, A. T. S. Wee, *Adv. Funct. Mater.* 2010, **21**, 410-424.
19 F. D'Souza, G. R. Deviprasad, M. E. Zandler, V. T. Hoang, A. Klykov, M. VanStipdonk, A. Perera, M. E. El-Khouly, M. Fujitsuka, O. Ito, *J. Phys. Chem. A* 2002, **106**, 3243-3252.
20 D. M. Guldi, N. Martin, Fullerenes: From Synthesis to Optoelectronic Properties. Springer Science Business Media Dordrecht, 2003.
21 F. Gao, O. Inganas, *Phys. Chem. Chem. Phys.* 2014, **16**, 20291-20304.
22 P. A. Lane, P. D. Cunningham, J. S. Melinger, G. P. Kushto, O. Esenturk, E. J. Heilweil, *Phys. Rev. Lett.* 2012, **108**, 077402-077407.
23 A. Sánchez-Díaz, L. Burtone, M. Riede, E. Palomares, *J. Phys. Chem. C* 2012, **116**, 16384-16390.
24 C. Schünemann, D. Wynands, L. Wilde, M. P. Hein, S. Pfützner, C. Elschner, K. J. Eichhorn, K. Leo, M. Riede, *Phys. Rev. B* 2012, **85**, 245314-245324.
25 S. Pfuetzner, C. Mickel, J. Jankowski, M. Hein, J. Meiss, C. Schuenemann, C. Elschner, A. A. Levin, B. Rellinghaus, K. Leo, M. Riede, *Org. Electron.* 2011, **12**, 435-441.
26 A. F. Bartelt, C. Strothkämper, W. Schindler, K. Fostiropoulos, R. Eichberger, *Appl. Phys. Lett.* 2011, **99**, 143304-143307.
27 D. M. Guldi, *Phys. Chem. Chem. Phys.* 2007, **9**, 1400-1420.
28 N. Sai, R. Gearba, A. Dolocan, J. R. Tritsch, W. L. Chan, J. R. Chelikowsky, K. Leung, X. Zhu, *J. Phys. Chem. Lett.* 2012, **3**16, 2173-2177.
29 J. Ren, S. Meng, E. Kaxiras, *Nano Research* 2012, **5**, 248-257.
30 J. Heyd, G. E. Scuseria, M. Ernzerhof, *J. Chem. Phys.*, 2006, **124**, 219906.
31 J. C. Tully, *Farad. Discuss.* 1998, **110**, 407-410.
32 D. Marx, J. Hutter, Ab Initio Molecular Dynamics: Basic Theory and Advanced Methods. *Cambridge University Press*, **2009**.
33 E. Runge, E. K. U. Gross, *Phys. Rev. Lett.* 1984, **52**, 997-1000.
34 M. A. Faist, T. Kirchartz, W. Gong, R. S. Ashraf, I. McCulloch, J. C. de Mello, N. J. Ekins-Daukes, D. D. C. Bradley, J. Nelson, *J. Am. Chem. Soc.* , 2012, **134**, 685-692.
35 A. Damjanovic, T. Ritz, K. Schulten, *Phys. Rev. B*, 1999, **59**, 3293-3311.
36 L. Blancafort , A. A. Voityuk, *J. Chem. Phys.* , 2014, **140**, 095102-095110.
37 E. P. Kenny, I. Kassal, *J. Chem. Phys. B* , 2016, **120**, 25-32.
38 X. Wu, H. Park, X. Y. Zhu, *J. Phys. Chem. C* 2014, **118**, 10670-10676.
39 D. E. Wilcox, M. H. Lee, M. E. Sykes, A. Niedringhaus, E. Geva, B. D. Dunietz, M. Shtein, J. P. Ogilvie, *J. Phys. Chem. Lett.* 2015, **6**, 569-575.
40 H. Phillips, Z. Zheng, E. Geva, B. D. Dunietz, *Org. Elect.* 2014, **15**, 1509-1520.
41 D. M. Guldi, A. Gouloumis, P. Vázquez, T. Torres, *Chem. Commun.* 2002, 2056-2057.
42 M. A. Loi, P. Denk, H. Hoppe, H. Neugebauer, C. Winder, D. Meissner, C. Brabec, N. S. Sariciftci, A. Gouloumis, T. Vázquez, P., Torres, T. *J. Mater. Chem.* 2003, **13**, 700-704.
43 D. M. Guldi, M. Prato, *Acc. Chem. Res.* 2000, **33**, 695-703.
44 G. Bottari, G. de la Torre, D. M. Guldi, T. Torres, *Chem. Rev.* 2010, **110**, 6768-6816.
45 S. Gadde, D. M. S. Islam, C. A. Wijesinghe, N. K. Subbaiyan, M. E. Zandler, Y. Araki, O. Ito, F. D'Souza, *J. Phys. Chem. C* 2007, **111**, 12500-12503.
46 V. Bandi, H. B. Gobeze, P. A. Karr, F. D'Souza, *J. Phys. Chem. C* 2014, **118**, 18969-18982.
47 S. Westenhoff, I. A. Howard, J. M. Hodgkiss, K. R. Kirov, H. A. Bronstein, C. K. Williams, N. C. Greenham, R. H. Friend, *J. Am. Chem. Soc.* 2008, **130**, 13653-13658.
48 J. M. Hodgkiss, A. R. Campbell, R. A. Marsh, A. Rao, S. Albert-Seifried, R. H. Friend, *Phys. Rev. Lett.* 2010, **104**, 177701-177705.
49 C. Yin, T. Kietzke, D. Neher, H. H. Horhold, *Appl. Phys. Lett.* 2007, **90**, 092117-092120.
50 F. Diederich, C. Thilgen, *Science* 1996, **271**, 317-324.
51 A. de la Escosura, M. V. Martínez-Díaz, D. M. Guldi, T. Torres, *J. Am. Chem. Soc.* 2006, **128**12 4112-4118.
52 A. L. Ayzner, D. Nordlund, D. H. Kim, Z. Bao, M. F. Toney, *J. Phys. Chem. Lett.* 2015, **6**, 6-12.
53 J. M. Soler, E. Artacho, J. D. Gale, A. Garcia, J. Junquera, P. Ordejon, D. Sánchez-Portal, *J. Phys.: Cond. Matt.* 2002, **14**, 2745-2779.
54 G. Kresse, J. Hafner, *Phys. Rev. B*, 1993, **48**, 13115-13118.
55 G. Kresse, J. Furthmüller, *Phys. Rev. B*, 1996, **54**, 11169-11186.
56 D. M. Ceperley, B. J. Alder, *Phys. Rev. Lett.* 1980, **45**, 566-569.
57 M. Dion, H. Rydberg, E. Schröder, D. C. Langreth, B. I. Lundqvist, *Phys. Rev. Lett.* 2004, **92**, 246401-246405.

58 P. E. Blöchl, *Phys. Rev. B*, 1994, **50**, 17953-17979.

59 G. Kresse, D. Joubert, *Phys. Rev. B* 1999, **59**, 1758âĂŞ1775.

60 N. Troullier, J. L. Martins, *Phys. Rev. B* 1991, **43**, 1993-2006.

61 J. Paier, M. Marsman, K. Hummer, G. Kresse, I. C. Gerber, J. G. Ańgyań, *J. Chem. Phys.* 2006, **124**, 154709-154722.

62 J. Paier, M. Marsman, G. Kresse, *J. Chem. Phys.* 2007, **127**, 024103-024113.

63 C. Franchini, R. Podloucky, J. Paier, M. Marsman, G. Kresse, *Phys. Rev. B* 2007, **75**, 195128-195139.

64 J. Heyd, G. E. Scuseria, M. Ernzerhof, *J. Chem. Phys.* 2003, **118**, 8207-8215.

65 A. Rubio, J. A. Alonso, X. Blase, L. C. Balbás, S. G. Louie, *Phys. Rev. Lett.* 1996, **77**, 247-250.

66 K. Yabana, G. F. Bertsch, *Phys. Rev. B* 1996, **54**, 4484-4487.

67 A. Tsolakidis, E. Kaxiras, *The J. Phys. Chem. A* 2005, **109**, 2373-2380.

68 S. Botti, A. Schindlmayr, R. Del Sole, L. Reining, *Rep. Prog. Phys.* 2007, **70**, 357-407.

69 Y. Tateyama, N. Oyama, T. Ohno, Y. Miyamoto, *J. Chem. Physics* 2006, **124**, 124507-124518.

70 J. C. Tully, *J. Chem. Phys.* 1990, **93**, 1061-1071.

71 I. Tavernelli, *Phys. Rev. B* 2006, **73**, 094204-094211.

72 I. Tavernelli, U. F. Rohrig, U. Rothlisberger, *Mol. Phys.* 2005, **103**, 963-981.

73 Y. Miyamoto, A. Rubio, D. Tomanek, *Phys. Rev. Lett.* 2006, **97**, 126104-126108.

74 J. Crank, P. Nicholson, *Proc. Camb. Phil. Soc.* 1947, **43**, 50-67.

75 L. Verlet, *Phys. Rev. B* **159**, *98*, 98-103.

76 T. Stein, J. Autschbach, N. Govind, L. Kronik, R. Baer, *J. Phys. Chem. Lett.* 2012, **3**, 3740-3744.

77 M. H. Lee, E. Geva, B. D. Dunietz, *J. Phys. Chem. C* 2014, **118**, 9780-9789.

78 G. Grunner, M. Dressel, *Electrodynamics of Solids: Optical Properties of Electrons in Matter*, Cambridge University Press: Cambridge, UK, 2012.

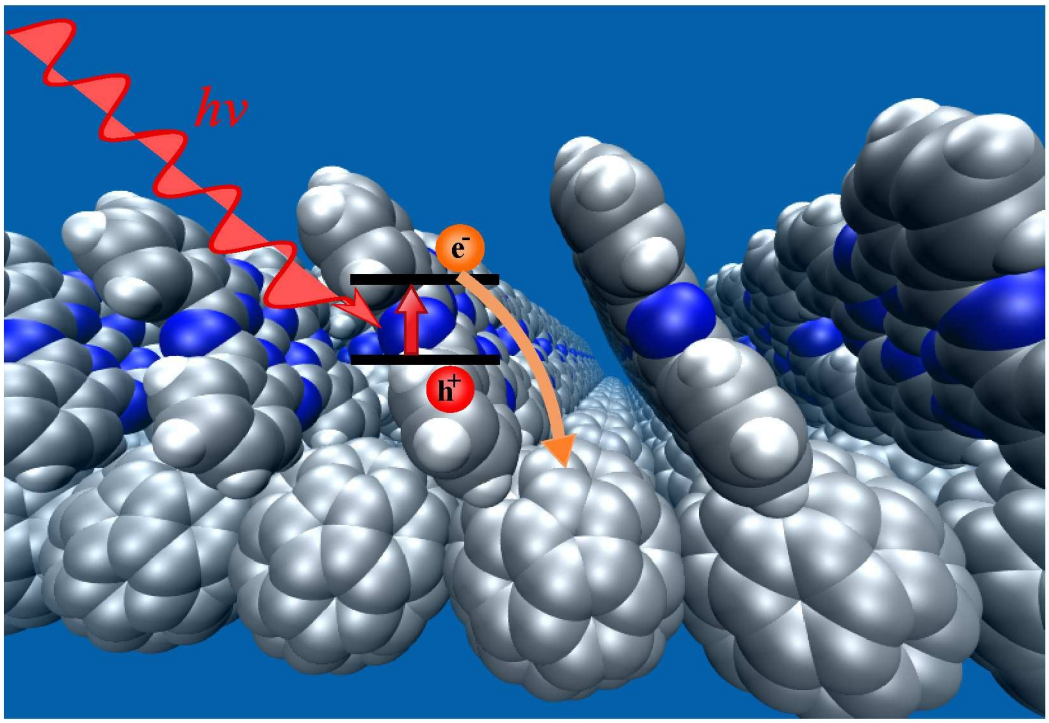


**FTOC 5** For Table of Contents Only.